RJC

RASĀYAN *J. Chem.*
Vol. 14 | No. 4 |2521-2528| October- December | 2021
ISSN: 0974-1496 | e-ISSN: 0976-0083 | CODEN: RJCABP
http://www.rasayanjournal.com
http://www.rasayanjournal.co.in

DETERMINATION OF THE EFFICIENCY OF HAFNIUM CARBIDE AND TANTALUM CARBIDE COATINGS DEPOSITED ON EXCHANGE MEMBRANE FUEL CELLS

C. Ruiz-Madera[1], J. Bautista-Ruiz[2] and W. Aperador[1,]✉

[1]Universidad Militar Nueva Granada, Bogotá, Colombia, 111101.
[2]Universidad Francisco de Paula Santander, San José de Cúcuta, Colombia, 540005.
✉Corresponding Author: g.ing.materiales@gmail.com

ABSTRACT

The energy efficiency of the hafnium carbide and tantalum carbide membranes (electrolyte) deposited through the PVD technique was determined from the systems simulation under operating conditions of parallel plates connected in series. Bipolar plates are used for two purposes: to conduct electrical current between the cells, and the other is to distribute hydrogen and oxygen. Thus, bipolar plates are used for two functions: one is to conduct electrical current between the cells, and the other is to distribute hydrogen and oxygen. We have developed two bipolar plate patterns, which include serpentine patterns and the bio-inspired flow field pattern. The coatings (serpentine) characterization was carried out using surface characterization techniques such as atomic force microscopy and structural identification by X-ray diffraction, allowing the analysis of the coating structure to determine the efficiency of carbide-based cathodes for hydrogen production from electrochemical impedance spectroscopy.

Keywords: Corrosion, Pitting, Leachates, Corrosion Rate, Membrane Fuel Cells

RASĀYAN *J. Chem.*, Vol. 14, No.4, 2021

INTRODUCTION

Hydrogen can operate in a closed cycle based on abundant and essential substances such as water or oxygen.[1] The hydrogen economy emerges from this idea because renewable energies are pretty complicated to transport.[2] The costs of the adverse effects and waste produced by these energies on the environment must be considered.[3] Energy companies have highlighted the versatility and viability of projects that include hydrogen as an energy source.[4] The water electrolysis is the most effective alternative to obtaining hydrogen without producing gases that contribute to the greenhouse effect.[5] Keeping in mind that hydrolysis is performed with different types of electrolyzers to obtain hydrogen, these developments are focused on comparing the efficiency between them and optimizing the development of new cathodes and the materials.[6] Studies are currently being conducted on carbide-type coatings for hydrogen production to replace high-cost materials with cheaper coatings that maintain physical, chemical, and electrocatalytic properties, advantages that have made coatings stand out today. Hafnium carbide (HfC) gained importance in the latest developments because it was found that this refractory ceramic can withstand scorching temperatures.[7]

Proton exchange membrane fuel cells (PEMFC) represent an alternative source of energy for transportation systems due to the absence of both air and noise pollutants, in addition to its high energy efficiency reaching an average of 0.5 W/cm^2 for a single cell.[8] An essential element in a fuel cell's performance is the channel flow pattern since it helps to evacuate the water generated during the electrochemical reaction and distribute the gases uniformly in the Membrane Electrode Assembly.[9,10]

In this research, the analysis of hafnium carbide and tantalum carbide layers deposited on exchange membranes is performed. Initially, a microstructural characterization is made using atomic force microscopy techniques and a structural identification by X-ray diffraction, allowing the coating structure's analysis. Then, the efficiency of carbide-based cathodes for hydrogen production will be determined by electrochemical impedance spectroscopy and simulated by computational fluid dynamics (CFD).

EXPERIMENTAL

Tantalum carbide TaC and hafnium carbide HfC layers were deposited on Nafion® composite membrane substrates by the non-reactive magnetron sputtering technique using an AJA-ATC 1800 system with a base

http://dx.doi.org/10.31788/RJC.2021.1446268
This work is licensed under a CC BY 4.0 license.

pressure of 10^{-7} Pa. Individual 2-inch diameter targets with a purity of 99.999% for the carbon (C) and 99.95% for the Tantalum (Ta) and Hafnium (Hf) targets are used for the deposition of the thin films, in a confocal configuration at a pressure of 0.4 Pa of argon.

To improve the carbide films' adherence, a metallic layer of Ta or Hf, either in the coating realized of about 30 nm of thickness, was deposited applying a power r.f. of 150 W to each target of Ta and Hf. Finally, TaC and HfC films with different compositions and thickness around 1 μm are deposited 70 W and 100 W for Ta and Hf targets, respectively, and maintaining the d.c. power to the carbon target fixed at 450 W.

The traditional British Bragg-Brentano geometry testing has been developed in a Panalytical Empyrean Diffractometer with a 240 mm incidence beam radius. The copper tube line presents a Kα1 of 1.540598 Å. The implemented potential difference was 40 kV with a current of 35 mA. The scanning range was from 10° to 100°. The step size assigned for this experiment was 0.04°, with a time count of 2 seconds for a total of 2125 points. A nickel filter is implemented in the incident beam to attenuate the Kβ, a 1° divergence grid, a 2° anti-dispersion grid, and a 0.04 rad soler grid. A receiving grid of 1⁄4°, an anti-dispersion grid of 1⁄2°, and a grid of 0.04 rad in the diffracted beam. The interpretation of the results was developed in the HighScore software with the PANalytical ICSD database.

The cells' performance was evaluated experimentally, using the electrochemical impedance technique (EIS). An electrochemical method was used to measure potential, time, and current, resulting in a series of impedance values for each frequency studied. EIS allows the efficient and assessed performance under practical conditions or denominated real; during the test, the cells always had a flow of hydrogen and oxygen symmetrically. The test temperature was 25 °C. This technique has been selected because it can relate physical, chemical, and mechanical properties with the electrical properties of materials and characterize their behavior and predict their life, assisting in improving these materials' manufacturing processes. In addition, EIS is a non-destructive technique, which can be used under hydrogen cell operating conditions. Impedance values were carried out by varying the frequency from 0.1 Hz to 30 kHz, with a data density of 5 points per decade. The applied alternate potential presents a sinusoidal behavior whose amplitude was 10 mV over the half-cell potential. After each experiment, the impedance data were plotted as Bode diagrams. From these plots with a high frequency, the total system impedance values are obtained. After the wear tests, the surface characterization implements a Nanosurf Flex-Axiom system atomic force microscope to analyze thin film surface topography. The measurement was performed in 46.2 μm x 46.2 μm using contact mode with aluminum-coated silicon tips. The measurements were made in three zones.

The simulation of the two types of patterns has been carried out to contrast the experimental results. In this case, the serpentine pattern is used to compare the proposed bio-inspired model. In Fig.-1, the two patterns used in the different simulations are illustrated.

(a) **(b)**

Fig.-1: (a) Serpentine Flow Pattern (b) Bio-inspired Flow Pattern

The serpentine channel has precisely one channel, requiring the remaining water's expulsion and the impurities present. However, the fluid must travel a long way, resulting in a pressure loss between the flow entrance and exit, generating a non-uniform distribution in the gas diffusion layer (GDL). The bio-inspired pattern seeks to improve energy efficiency without producing higher pressure losses than with the serpentine pattern.[11,12] Additionally, the use of hafnium carbide and tantalum carbide deposited as a variant for the membrane (electrolyte) is also proposed to generate a higher power density. The simulation has been performed utilizing computational fluid dynamics (CFD) using the COMSOL Multiphysics® Modeling Software. All components of a fuel cell are taken into account for the simulation.[13]

RESULTS AND DISCUSSION

Figure-2 shows the HfC and TaC coatings characterization results by X-ray diffraction (XRD), which were deposited on a Nafion® composite membrane. Nowadays, the coatings are made to leave a weak layer, but it maintains their characteristics. XRD obtained the crystallographic structure of HfC, and TaC coatings, Fig.-2(a) and Fig.-2(b) show respectively the X-ray pattern, the crystallographic structure of the HfC coating illustrated in Fig.-2(a), showed the presence of HfC with an agreement at 33.571°, and a cubic structure with a crystalline plane (111), and at 70.25° with a cubic structure and an orientation at (222). Figure-2(b) shows the diffractogram for the TaC sample. The crystalline phases were identified: at 40.48 ° tetragonal phase to the plane (020), and at 34.87°, 59.01° and 69.33° cubic structure according to crystalline planes (111), (022), and (113), respectively. These results are in agreement with other investigations.[26]

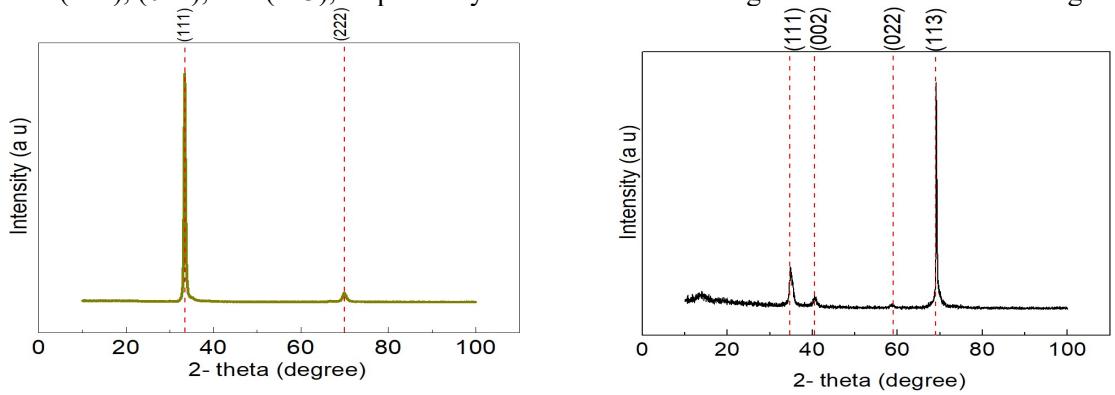

(a) (b)

Fig.-2: X-ray Diffraction Patterns for the Thin Films of (a) HfC and (b) TaC.

The micrographs obtained by atomic force microscopy are observed in Fig.-3(a) and Fig.-3(b), which shows the surface characterization of the hafnium carbide sample in whom the characterized surface showed the topographic heterogeneity.[14] It is possible to observe a value of 645 nm, coating relating the average roughness and corresponding to the thin film. In observing the different zones, no surface affectation is appreciated, so in the oxide-reduction processes, an adequate chemical reaction will be obtained, generating a suitable device as an essential part of the cell. Concerning the micrography corresponding to tantalum carbide, a value of 30.3 nm is obtained, it is a smoother surface, and the area allows indicating that the energy distribution is homogeneous. The TaC coating presented the most uncomplicated response in terms of the surface because this is a stronger bond. That is why it presents a more compact system about HfC.[14] In Fig.-4, the Nyquist diagrams are displayed. For the cells where the thin films of HfC and TaC are in the form of a membrane, four resistances are observed, and three constant phase elements, these parameters were calculated from the equivalent circuit in Fig.-5. The values of each element are detailed in Table-1. Rp is the concentration of the ions present in the cell. Its value is low because the evaluation temperature has been 25°C. R1 is related to the proton membrane and the electrical resistance of the plates. R2 is associated with the load transfer resistance at the anode and concerns hydrogen's transfer resistance or oxidation reaction. R3 is associated with the load transfer resistance at the cathode, where oxygen reduction is performed.[15,16]

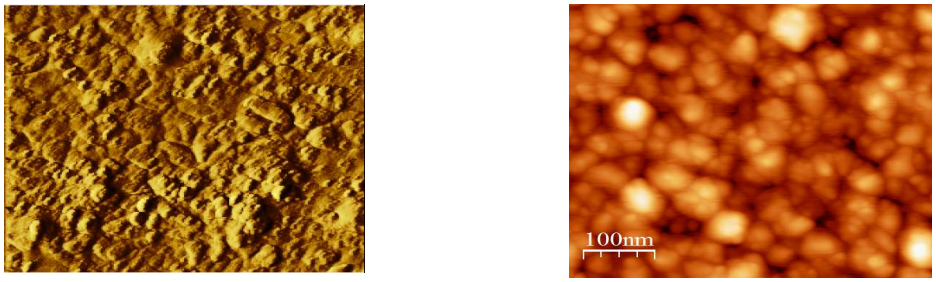

(a) (b)

Fig.-3: Atomic Force Microscopy Images of (a) HfC and (b) TaC Coatings

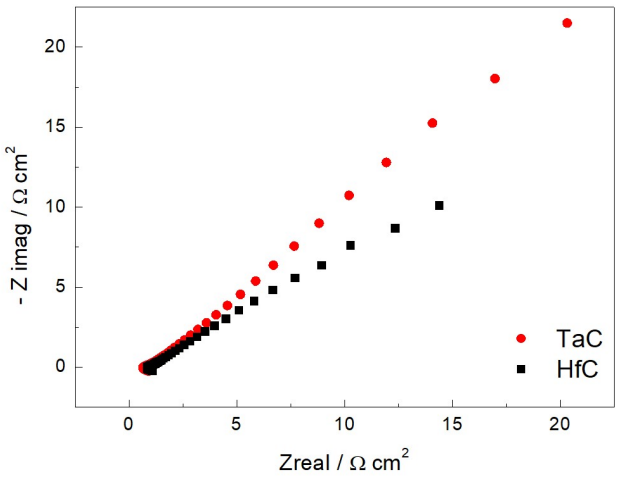

Fig.-4: Nyquist Diagram of HfC and TaC Coatings

The carbide-based cathode efficiency for hydrogen production is obtained through the equivalent circuit parameters, so it was determined that the TaC generates a higher performance compared to the HfC. These results are obtained by connecting the cell to a gaseous flux, so the membranes have a permanent ionic passage and a hydration process is generated. Where it is obtained, there is less permeability for the TaC membrane since the resistance value of the proton membrane is increased with the HfC.[17] The resistances' superior values directly correlate with the topography obtained by atomic force microscopy, with a diffusion layer process, which generates a better passage of electric current.[18,19]

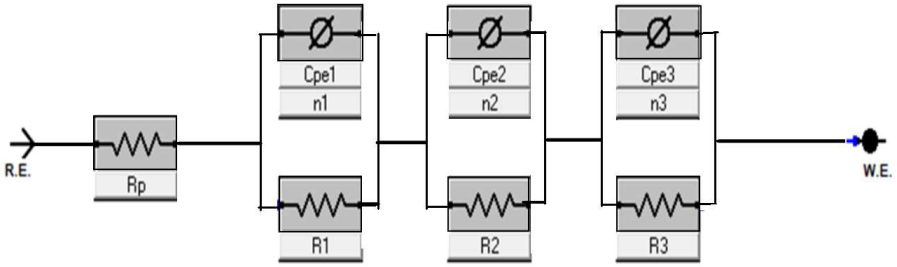

Fig.-5: Equivalent Circuit

Table-1: Parameter Values for Equivalent Circuit Elements for HfC and TaC Coatings

	Rp	R_1	R_2	R_3	CPE_1	n_1	CPE_2	n_1	CPE_3	n_3
HfC	0.0032	0.21	2.32	42.32	0.0721	0.72	0.7982	0.82	0.8231	0.85
TaC	0.0021	0.14	1.87	15.21	0.0325	0.83	0.7023	0.94	0.7821	0.95

Simulation

Computer Models

Flux through the fuel cell is assumed to be laminar, stable, and incompressible. The temperature remains constant, i.e., isothermal. The Brinkman equations determine the gas diffusion layer flow and mass transport (Eq.-1 and Ed.-2). In the flow pattern (Fig.-1), the fluid is represented by the equations of Navier-Stokes (Eq. 3

$$\left(-\nabla * \frac{\eta}{\varepsilon}(\nabla \mathrm{u} + (\nabla \mathrm{u})^T)\right) - \left(\frac{\eta}{k}u + \nabla \mathrm{p} - \mathrm{F}\right) = 0 \quad (1)$$

$$\nabla * \mathrm{u} = 0 \quad (2)$$

$$\frac{\partial \mathrm{u}}{\partial \mathrm{t}} + u * \nabla \mathrm{u} = -\frac{\nabla \mathrm{P}}{\rho} + v\nabla^2 u \quad (3)$$

Where ρ is density (kg/m^3), η is dynamic viscosity (kg/(ms)), u is velocity vector (m/s), p is pressure (Pa), ε is porosity, k is permeability (m^2). F refers to the influence of gravity small effects that are not taken into account for this case.

Frontier Conditions

Four boundary conditions have been generated for each simulation.

1. Cell component conditions where Brinkman's (Eq.-1 and Eq.-2) and Navier Stokes' (Eq.-3) equations are applied for fluids in porous media
2. Input conditions in which the type of fluid (oxygen and hydrogen) and its velocity are defined.
3. Output conditions with atmospheric pressure as output pressure.
4. Wall boundary conditions, in which there is the condition of no sliding.

The membrane has a thickness of 100 µm, and the GDL has a thickness of 50 µm. The other parameters of the simulation can be seen in Table-2.

Table-2: Variables for the Simulation.

Unit	Value	Description
$\boldsymbol{\varepsilon}$	0.4	GDL Porosity
k (m^2)	1.18e^{-11}	GDL Permeability
σ (S/m)	222	Electrical conductivity of GDL.
wH_2	0.74	Mass fraction of hydrogen
wH_2O	0.03	Waterbody fraction
wO_2	0.23	Oxygen mass fraction
Vin (m/s)	0.5	Input rate
T (K) (°C)	80 - 353	Fuel cell temperature
V (v)	0.9	Cell voltage

The simulation provides current density distribution, fluid distribution throughout the flow channel, and pressure decreases for the serpentine pattern and the bio-inspired flow and changes the electrolyte between Nafion, HfC, and TaC. Fluid (Fig.-6 and Fig.-7a) and pressure drops (Fig.-6 and Fig.-7b) change between two proposed patterns but do not show a notable variation with changing of the electrolyte.

The pattern with serpentine and Nafion as the electrolyte is the base point for analysis. According to Fig.-8, a maximum of 5.7x10^3 A/m^2 is obtained, equivalent to 0.513 W/cm^2, considering a voltage of 0.9 V, a value consistent with that indicated previously.[20] The bioinspired pattern has a slight increase in pressure losses due to decreased fluid velocity and pattern. This decrease is a consequence of the more extended channel in the bioinspired model. Additionally, higher current density values are evident. Figure-8 shows that the magnitude of the current density improves by 8.1% using Nafion as an electrolyte concerning 4.5% due to pressure loss.

(a) (b)

Fig.-6: Results of the Serpentine Structure (a) Distribution of the Fluid in the Flow Channel, (b) Pressure Losses

The primary improvement is obtained by changing the membrane, where the pressure drops are maintained, but there is a considerable increase in current density for both flow patterns. The same pressure losses are maintained for hafnium carbide, but they generate 10.9% and 10.6% higher current density for the serpentine and bio-inspired pattern. Fig.-9(b) shows a 7.8% more current

density than the serpentine pattern. The TaC was the best performing electrolyte with 15.4% higher energy efficiency for the serpentine and 15.3% higher for the bio-inspired pattern, as seen in Fig.-10.

(a) (b)

Fig.-7: Bio-inspired Pattern. (a) Distribution of the Fluid in the Flow Channel, (b) Pressure Losses.

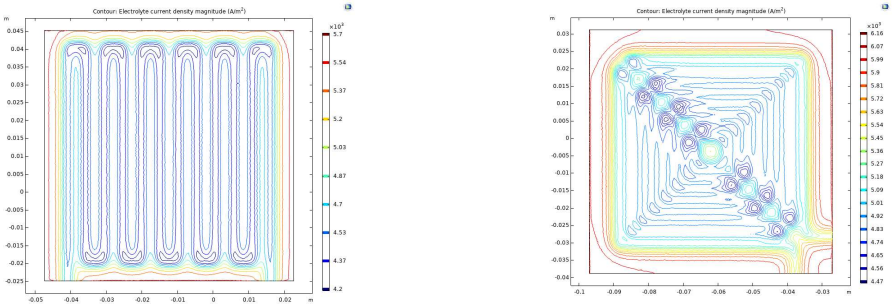

(a) (b)

Fig.-8: Current density using Nafion as the electrolyte. (a) Serpentine. (b) Bio-inspired pattern.

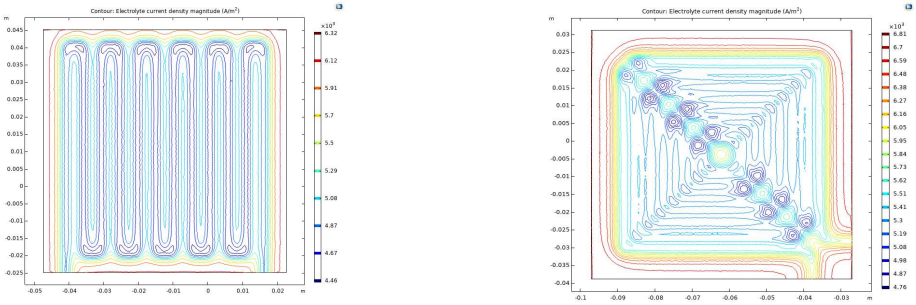

(a) (b)

Fig.-9: The Current Density with HfC as the Electrolyte. (a) Serpentine. (b) Bio-inspired Pattern

Overall, the bio-inspired pattern and new membrane materials reflect a significant improvement in fuel cell energy efficiency.[20] Some modifications to the bio-inspired flow can be made to reduce pressure losses, including parallel pathways for more uniform distribution. Fig.-11 provides a visualization of the data obtained from the simulation.[20]

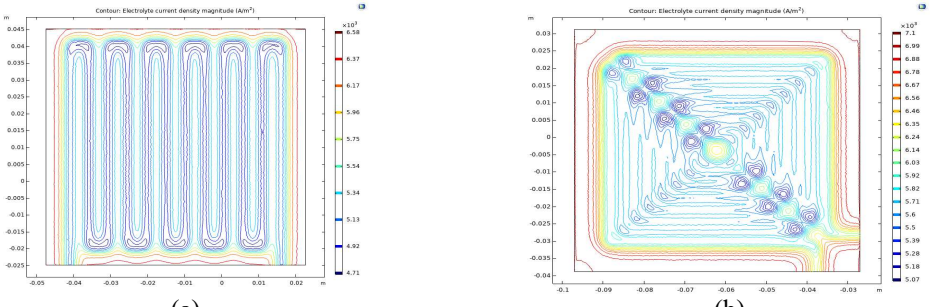

(a) (b)

Fig.-10: The Current Density with TaC as the Electrolyte. (a) Serpentine. (b) Bio-inspired Pattern

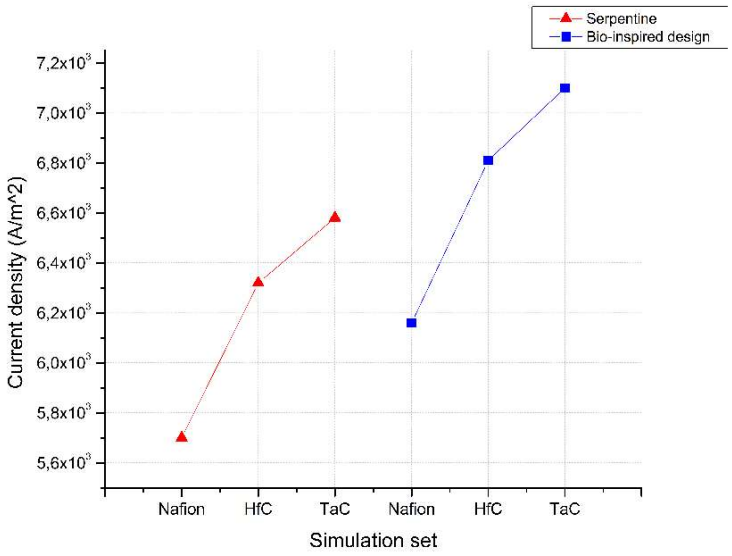

Fig.-11: Current Density in Different Fuel Cell Configurations

CONCLUSION

Hafnium carbide and tantalum carbide coatings demonstrated their potential use as electrodes in hydrogen production due to their efficient electrocatalytic activity. The micrographs obtained by atomic force microscopy are observed, which shows the surface characterization of the hafnium carbide sample in whom the characterized surface showed the topographic heterogeneity. For the cells where the thin films of HfC and TaC are in the form of a membrane, four resistances are observed, and three constant phase elements, these parameters were calculated from the equivalent circuit. The carbide-based cathode efficiency for hydrogen production is obtained through the equivalent circuit parameters, so it was determined that the TaC generates a higher performance compared to the HfC.

ACKNOWLEDGEMENT

This research was funded by the Universidad Militar Nueva Granada, a Product derived from the IMP ING 3123 research grant 2020-2021

REFERENCES

1. K. Ahmad, H.R. Ghatak and S.M. Ahuja, *Environmental Technology & Innovation*, **19**, 100893(2020), https://doi.org/10.1016/j.eti.2020.100893
2. A.G. Stern, *International Journal of Hydrogen Energy*, **40(32)**, 9885(2015), https://doi.org/10.1016/j.ijhydene.2015.05.111
3. C.J. Winter, *International Journal of Hydrogen Energy*, **34(14)**, 1(2009), https://doi.org/10.1016/j.ijhydene.2009.05.063
4. S. Jyothi, Y.V. Subba Rao and P.S. Samuel Ratnakumar, *Rasayan Journal of Chemistry,* **12(2)**, 537 (2019), https://doi.org/10.31788/RJC.2019.1225000
5. J. Bautista-Ruiz, W. Aperador and J.J. Olaya*, Rasayan Journal of Chemistry,* **11(2)**, 597(2018), https://doi.org/10.31788/RJC.2018.1122075
6. Y. Zhou, W. Wang, C. Zhang, D. Huang, C. Lai, M. Cheng, L. Qin, Y. Yang, C. Zhou, B. Li, H. Luo and D. He, *Advances in Colloid and Interface Science*, **279**, 102144(2020), https://doi.org/10.1016/j.cis.2020.102144
7. P. Valencia, L. Yate, W. Aperador, Y. Li, and E. Coy, *The Journal of Physical Chemistry C*, **122(44)**, 25433 (2018), https://doi.org/10.1021/acs.jpcc.8b08123
8. T. Demirdelen, F. Ekinci, B.D. Mert, İ. Karasu and M. Tümay, *International Journal of Hydrogen Energy*, **45(18)**, 10680 (2020), https://doi.org/10.1016/j.ijhydene.2020.02.007

9. R. Thilagavathi, A. Prithiba and R. Rajalakshmi, *Rasayan Journal of Chemistry*, **12(2)**, 431(2019), https://doi.org/10.31788/RJC.2019.1225133
10. Z. Huang, J. Shen, S.H. Chan and Z. Tu, *Energy Conversion and Management*, **226**, 113492(2020), https://doi.org/10.1016/j.enconman.2020.113492
11. H. Yuan, H. Dai, X. Wei and P. Ming, *Journal of Power Sources,* **468**, 228376(2020), https://doi.org/10.1016/j.jpowsour.2020.228376
12. A. Ozden, M. Ercelik, D. Ouellette, C. Ozgur-Colpan, H. Ganjehsarabi and F. Hamdullahpur, *International Journal of Hydrogen Energy*, **42(33)**, 21546(2017), https://doi.org/10.1016/j.ijhydene.2017.01.007
13. R. Roshandel, F. Arbabi, and G. Karimi Moghaddam, *Renewable Energy*, **41**, 86(2012), https://doi.org/10.1016/j.renene.2011.10.008
14. M.Z. Chowdhury and B. Timurkutluk, *Energy*, **161**, 104(2018), https://doi.org/10.1016/j.energy.2018.07.143
15. J. Zhang, Y. Zhang, Y. Fu, T. Li, and J. Meng, *Vacuum,* **169**, 108886(2019), https://doi.org/10.1016/j.vacuum.2019.108886
16. G. Feng, H. Li, X. Yao, D. Hu, L. Yang, B. Li and J. Lu, *Surface and Coatings Technology*, **400**, 126219(2020), https://doi.org/10.1016/j.surfcoat.2020.126219
17. C.G. Lee, *Journal of Electroanalytical Chemistry*, **810**, 48(2018), https://doi.org/10.1016/j.jelechem.2018.01.005
18. S. Chen, W. Xiong, Z. Yao, G. Zhang, X. Chen, B. Huang, and Q. Yang, *International Journal of Refractory Metals and Hard Materials*, **47**, 139(2014), https://doi.org/10.1016/j.ijrmhm.2014.07.010
19. M. Hosseini, H.H. Afrouzi, H. Arasteh, and D. Toghraie, *Energy*, **188**, 116090(2019), https://doi.org/10.1016/j.energy.2019.11609
20. J. P. Kloess, X. Wang, J. Liu, Z. Shi, and L. Guessous, *Jounal of Power Sources*, **188(1)**, 132(2009), https://doi.org/10.1016/j.jpowsour.2008.11.123

[RJC-6268/2020]